On the gelation of humins: From transient to covalent networks

Kenneth Cerdan[1], Jesus Gandara-Loe[2], Giel Arnauts[2], Vedran Vangramberen[1], Anton Ginzburg[3], Rob Ameloot[2], Erin Koos[1], Peter Van Puyvelde[1]*

[1] Department of Chemical Engineering, Soft Matter, Rheology and Technology (SMaRT), KU Leuven, Celestijnenlaan 200J, 3001 Heverlee, Belgium
[2] Department of Microbial and Molecular Systems, Centre for Membrane Separation, Adsorption, Catalysis and Spectroscopy, KU Leuven, Celestijnenlaan 200J, 3001 Heverlee, Belgium
[3] Department of Chemical Engineering, Soft Matter, Rheology and Technology (SmaRT), Wetenschapspark 27, 3590 Diepenbeek, Belgium

* Corresponding author: kenneth.cerdangomez@kuleuven.be

Keywords: Gelation, humins, rheology, gels, transient network, covalent network, carbonaceous gel, viscosity, viscoelasticity

Abstract

Humins are a by-product of many acid-catalyzed biorefinery processes converting polysaccharides into platform chemicals. The valorization of humins residue to increase the profit of biorefinery operations and reduce waste is a field that is growing interest as the production of humins continues growing. This includes their valorization in materials science. For a successful processing of humins-based materials, this study aims to understand the thermal polymerization mechanisms of humins from a rheological perspective. Thermal crosslinking of raw humins leads to an increase in their molecular weight, which in turn leads to the formation of a gel. Humins gels structure combine physical (thermally reversible) and chemical (thermally irreversible) crosslinks, and temperature plays an essential role on the crosslink density and the gel properties. High temperatures delay the formation of a gel due to the scission of physicochemical interactions, drastically decreasing their viscosity, whereas upon cooling a stronger gel is formed combining the recovered physicochemical bonds and the newly created chemical crosslinks. Thus, a transition from a supramolecular network to a covalently crosslinked network is observed, and properties such as the elasticity or reprocessability of humins gels are influenced by the stage of polymerization.

1 Introduction

Humankind's flawed use of resources yields a severe ecological footprint to the detriment of our planet's welfare. The current situation has reached a tipping point where the growing environmental concerns demand from society to urgently shift towards other sustainable alternatives to restrain the mismanagement of available resources. The chemical industry is currently engaging this situation implementing more sustainable solutions and processes relying on the 12 Green Chemistry Principles proposed by Anastas and Warner[1]. Industrial developments towards sustainability rely on the efficient and responsibly scalable use of renewable resources to replace fossil-based products, as well as appropriate valorization routes for the generated waste by-

products[2]. An example to accomplish this task is addressed by Avantium (The Netherlands), who are making breakthroughs towards the sustainable production of polyethylene furanoate (PEF) as an excellent plant-based substituent of fossil-based polyethylene terephthalate (PET)[3]. Many biorefinery processes that approach this transition find acid-catalyzed treatments of lignocellulosic biomass as a promising route to obtain versatile platform molecules such as 5-hydroxymethylfurfural (HMF) or levulinic acid (LA)[4-7].

A severe drawback of many biorefinery processes is the inevitable formation of undesired products referred to as humins. Humins are dark, highly viscous, polydisperse and poorly soluble carbonaceous by-products produced by random polymerization processes during the acid-catalyzed dehydration of polysaccharides. Their formation reduces the yield of the desired products, hindering the economic viability of many biorefinery processes. In addition, other issues such as reactor clogging and catalyst poisoning due to the adsorption and growth of humins on the surface also limits the operational effectiveness in the long-term[8, 9]. The mapping of the chemical structure of humins, as well as identifying their formation pathways to aid in the design of prevention strategies, are growing research fields striving to avert biorefineries revenue depletion[8, 10-17].

Regardless of these efforts, the formation of humins is ubiquitous. In this regard, their post-treatment to be converted into added-value products such as fuels[18], printing inks[19] or adhesives[20] has been recently explored. Moreover, the use of raw humins as a feedstock for the preparation of new materials is a particularly promising route due to its simplicity and straightforward applicability. Polymeric materials such as porous foams[21-24], thermoset resins[25-27], elastomers[28] or polymer blends[29] have been investigated for value-added applications including capacitors[30], binders[31], catalysis[32, 33], adsorbents[34, 35], reinforced composites[36, 37] or self-healing robotics[29].

As described above, humins are becoming an increasingly popular choice for the preparation of novel polymeric materials. However, their processability for such applications is still poorly understood. This is of paramount importance to reproducibly prepare materials with the best performance. The formation mechanisms of humins consist of the oligomerization of HMF derivates and subsequent nucleation and growth as insoluble particles with polydisperse molecular weight (M_w). An increased degree of polymerization turns humins into solid brittle products similar to biochar. Several studies involving calorimetry[38] or x-ray scattering[39] clarified this growth process, albeit more information is needed to assess the utility of humins in the polymer processing field. The rheological properties of humins, however, remains poorly understood and can prompt a more detailed understanding of their polymerization. A particularly interesting process in the growth of humins is the gel transition, that is, the evolution from a flowing viscous state to an interconnected solid network. The gel transition is strongly influenced by the microstructural evolution of reacting humins and the nature of the interactions participating in the process. For this purpose, rheology is proven to be a powerful tool to inspect the gel point as a result of the drastic change in elasticity as the network percolates.

The goal of this research is to perform a detailed evaluation of the gelation process of humins focusing on the use of calorimetric and rheological tools. The identification of the gelation mechanisms aids the prediction of the rheological and mechanical response of humins upon processing. This is directly related to the performance of the resulting humin-derived materials. Based on previous studies reporting tempting application routes, the covalent crosslinking of humins is mostly (but not exclusive) due to aldol condensation reactions between furanic oligomers[13, 40], leading to the formation of colloidal particles that eventually percolate in a gel network[39]. However, the presence of abundant oxygenated groups as well as adsorbed low M_w hydrophilic molecules leads to the formation of cohesive physical interactions between particles such as hydrogen bonds and Van der Waals interactions, respectively[11, 41]. These physical interactions dominate the humins' viscoelastic properties and increasing the covalent crosslinking density decreases in their impact in the final network properties. Thus, we observed a transition from a Newtonian liquid to a physical gel, eventually evolving towards the formation of a chemical gel as the polymerization reactions proceed. In addition, humins can undergo thermo-reversible gelation when present as a physical gel, which is of utmost importance for the preparation of reprocessable materials.

2 Materials & Methods

2.1 Materials

Humins were supplied by Avantium Renewable Chemicals BV and used as received. Humins were sealed and stored at 20 ˚C to prevent any potential alteration of their properties such as moisture adsorption, side reactions or residual contamination throughout the development of this study.

2.2 Methods

2.2.1 FT-IR

The effect of the temperature on the chemical composition of humins was evaluated by IR spectroscopy using a bespoke IR sandwich cell similar to those reported previously in literature [42]. The desired amount of humins was placed in a Ø = 16 mm double-sided polished Si wafer and exposed to a 40 mL/min N_2 flow. IR spectra were collected at room temperature, 30, 40, 50, 60 and 80 ˚C using a 3 ˚C/min ramp and kept isothermal at each temperature for 15 min with a Varian 670 FT-IR spectrometer (64 scans/spectrum) equipped with an MCT detector.

2.2.2 TGA-MS

TGA was carried out on a NETZSCH STA 449 F3 Jupiter® instrument in synthetic air atmosphere (80% nitrogen/20% oxygen) flowing at a rate of 50 mL/min. After evacuating the TGA chamber, about 100 mg of the humins contained in alumina crucibles was heated up to 60, 80 and 100 ˚C at a rate of 10 ˚C/min and held at the respective temperature for 5 hours. To compensate for the buoyancy effect, the weight decrease of an empty crucible under identical conditions is subtracted from the measured data. During the heating step, the outlet of the TGA was connected to a Hiden HPR-20 QIC – EGA mass spectrometer via a high-purity alumina sampling tube. Ions

related to the release of water (m/z = 18) and HMF (m/z = 41, 97, 126) were recorded. A Savitzky-Golay filter (100 points) was applied to the signal of HMF (m/z = 97) to reduce noise.

2.2.3 Differential Scanning Calorimetry

The glass transition temperature (T_g) of raw humins and thermally treated humins was monitored by Differential Scanning Calorimetry (DSC) using a Q2000 DSC (TA Instruments) equipped with a Refrigerated Cooling System (RCS). A 25 mL.min^{-1} N_2 gas flow was used to purge the DSC cell. Humins samples (5 – 10 mg) were loaded into 100 µL T_{zero} aluminum DSC pans and submitted to a cooling/heating cycle. This cycle consists on a temperature ramp of 10 ˚C/min over a temperature range of (–80 ˚C) – 60 ˚C.

2.2.4 Rheological Measurements

Rheological experiments were performed both under rotation and oscillation on an AR-G2 rheometer (TA Instruments). The rheometer was equipped with an ETC heating system under air atmosphere to control the chamber temperature during the measurements. Humins were placed on disposable 40 mm aluminum parallel plates, keeping a consistent measurement gap of 1 mm. Humins were loaded by first heating them up to 50 ˚C in the rheometer to lower their viscosity enough to achieve an intimate contact with the plates. Upon loading and trimming the sample excess, humins were cured at temperatures over the range of 25 ˚C – 100 ˚C depending on the desired experiment. To avoid testing errors, all the experiments were repeated for a minimum of three reproducible times.

Flow sweeps under rotation were performed with an apparent shear rate increasing from 0.01 s^{-1} to 100 s^{-1} over the temperature range of 25 ˚C – 100 ˚C. Samples were equilibrated for 5 minutes before starting the test. Low and high shear rates were adapted for samples at low and high temperatures that exceed the instrument torque limitations.

Oscillatory rheological experiments were performed under controlled strain. Humins viscosity determination under oscillation was carried out within the same temperature range as the flow sweeps but performing oscillation frequency (ω) sweeps within the frequency range from 0.1 Hz to 100 Hz. Humins gelation was approached using two different methods investigating the evolution of the rheological viscoelastic properties as a function of temperature (60 ˚C – 100 ˚C): (i) Isothermal experiments continuously monitoring the evolution of the storage (G') and loss ($G"$) modulus at a constant temperature over a wide timeframe. (ii) Stepwise experiments, first conditioning humins to let them react at a certain temperature and time, measuring the resulting viscoelastic parameters upon cooling at room temperature. The strain values used were previously confirmed to be present in the linear viscoelastic region (LVR) and adjusted to each experiment based on the used temperature, ranging from 0.1 % to 1 %, at a frequency of 1 Hz.

In this study, the determination of the gel point is reported following two different approaches: (i) For the determination of the quiescent critical gel time, the gel point is pragmatically reported as the $G'(T)$ and $G"(T)$ crossover point at a single frequency of

1 Hz. (ii) For non-quiescently gelled humins, the influence of the frequency on the critical gel viscoelastic properties is considered being the gel point the point where the loss angle $\tan(\delta)$ becomes frequency independent and the viscoelastic moduli follow a power law. In addition, the frequency dependence of humins' viscoelastic properties at the different gelation stages was assessed performing oscillation frequency sweeps between 0.1 Hz and 100 Hz at room temperature following the same approach as the gelation stepwise experiments.

Reverse gelation tests of humins gels were carried out under dynamic oscillation using two different approaches. First, thermal degelation is achieved by steadily increasing the temperature of humins from 25 ˚C to 140 ˚C at a heating rate of 1 ˚C/min. Initially, humins were pre-conditioned at 100 ˚C during a timescale of 15 – 60 min to assess the influence of covalent crosslinks on the process. A strain value of 0.01% and five discrete frequencies (0.3 Hz, 0.6 Hz, 1 Hz, 1.8 Hz, 3.1 Hz) were used for this purpose. The loss angle crossover point where its value is frequency independent is determined to be the gelation point. A cooling ramp under the same conditions is subsequently performed to evaluate the reversibility of the gelation process. Second, the rejuvenation of humins gels followed by the gel recovery was tested under shear at two different amplitudes. A low strain amplitude of 0.1%, within the linear viscoelastic regime, is applied to humins previously stabilized at 50 ˚C to measure the resulting viscoelastic properties. Subsequently, humins were submitted to a large strain amplitude value of 10% to collapse their structure. After this process, humins were allowed to both recover and cure by conditioning them at 100 ˚C for 10 minutes, being subsequently cooled back to 50 ˚C and equilibrated for 10 more minutes. The same cyclic loading and curing was repeated for six times.

3. Results & Discussion

3.1 Chemical and thermal Analysis of Isothermally Treated Humins

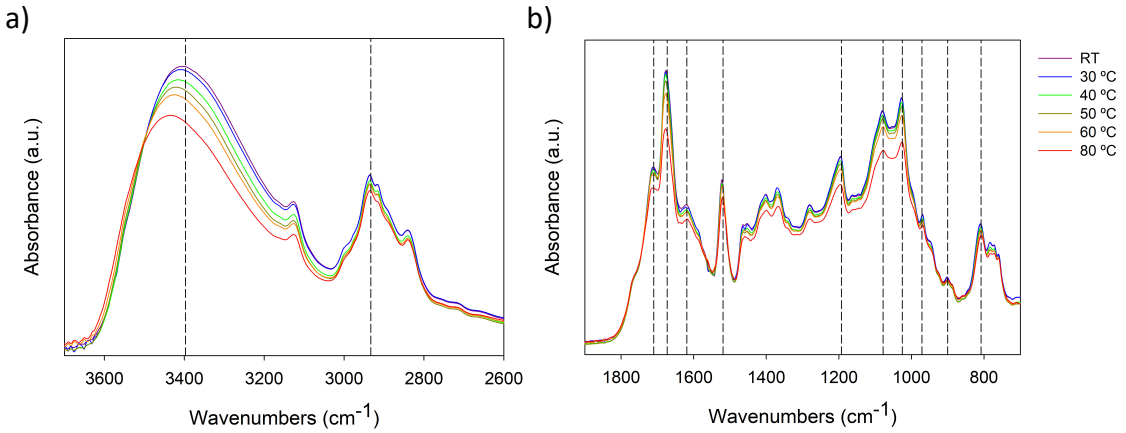

Figure 1. FT-IR spectra of humins at different temperatures under N_2 atmosphere (15 minutes isothermal at each temperature for the displayed scans) in the range of a) 3700 – 2600 cm^{-1} and b) 1900 – 700 cm^{-1}.

Table 1. Assignment of the major IR peaks of humins.

Assignment	**Wavenumber (cm^{-1})**
-OH stretching	3397
-CH aliphatic stretching	2933
C=O conjugated to alkene	1710
C=O group in HMF humins	1673
C=C stretching conjugated with C=O	1619
C=C stretching furan rings	1519
HMF	1193
C-H bending furan ring	1078
C-O stretching, furan ring/humins	1025
=C-H *trans*	971
=C-H *cis*	900
C-H out of plane deformation, furan ring	808

Figure 1 shows the FT-IR spectra of humins treated at temperatures in the range of 25 – 80 ˚C under N_2 atmosphere, and the peaks assignments are summarized in **Table 1**. **Figure 1a** focuses on the 3700 – 2600 cm^{-1} region by displaying the -OH (*ca.* 3390 cm^{-1}) and -CH (*ca.* 2900 cm^{-1}) stretching modes. The analyzed samples experience a decrease tendency for all the showed bands which can be attributed to a mild evaporation of humins when heated. The relative intensity of these two peaks changes significatively by increasing the temperature. The -OH and the -CH stretching peaks intensities decrease, thus evidencing chemical modifications occurring due to changes in temperature. Furthermore, the shift of the vibrational -OH stretching suggests the presence of different -OH groups and the modification of hydrogen bonds when increasing the temperature [36]. More precisely, a decrease of the -OH peak intensity is translated in this case into a decrease in concentration of hydrogen bonds. **Figure 1b**, which focuses on the 1900 – 700 cm^{-1} range, displays a drastic decrease of the peaks attributed to HMF at 1673 and 1025 cm^{-1}. This also confirms the crosslinking of raw humins. It can also be observed that the 1673 cm^{-1} peak presents two additional shoulders at 1710 cm^{-1} and 1619 cm^{-1}. The presence of these two additional peaks are indicators of the presence of species derived from HMF, which can be the result of the polymerization of HMF or their incorporation into the structure of humins. Finally, the peaks observed at 971 cm^{-1} and 900 cm^{-1}, corresponding to the *trans* and *cis* configurations of double bonds, respectively, exhibit a different behaviour. Whereas the *trans* signal follows the decrease tendency of rest of the bands, maybe due to the evaporation of humins components, the *cis* peak remains unaltered. This is due to the generation of new double bonds created during the polymerization of humins[10]. Hence, the loss of *cis* bonds during the evaporation of humins is compensated by the formation upon crosslinking of new *cis* double bonds, being more stable than the *trans* counterpart, possibly due to steric hindrance

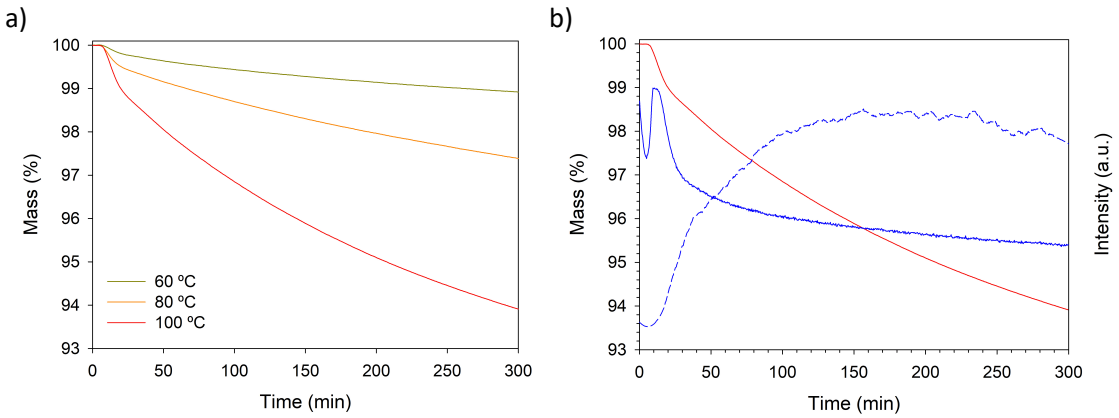

Figure 2. a) TGA of humins heated at an isothermal stage of 5 hours at 60 ˚C (dark yellow), 80 ˚C (orange) and 100 ˚C (red). b) TGA-MS (TGA and MS results corresponds to the red and blue profiles, respectively) of humins: Water (m/z = 18, solid blue line) and HMF (m/z = 97, dashed blue lines) intensities are displayed after normalization.

To support the hypothesis on the polymerization of humins, TGA-MS was performed to monitor the volatile compounds released while heating the sample. After a short dynamic heating step, three samples were kept at isothermal stages of 60, 80 and 100 °C for 5 hours (**Figure 2a**). Due to a thermal mismatch between the oven and the sample thermocouple, a small overshoot in sample temperature can be observed before a stable equilibrium temperature is adopted. For all measurements, an initial quick weight decrease is followed by a slower decline as soon as the isothermal heating temperature is established. The deceleration of the weight loss scales with the temperature of the isothermal step and indicates a continuous release of one or more compounds. By coupling the exhaust of the TGA to a mass spectrometer, these species could be identified. Since similar trends were observed for TGA-MS measurements at the three temperatures, one experiment, *i.e.* the measurement at 100 °C, was selected to demonstrate the release of different compounds. The evolution of ion fragments related to release of water (m/z = 18) and HMF (m/z = 97) are displayed in **Figure 2b**, together with the TGA curve. After initial decrease of signal intensity (as a consequence of baseline drift), water and HMF signals start to increase after 5 minutes, when the sample temperature is approximately 60 °C. The mass peak of water around 10 – 15 minutes suggests that the formation of water as byproduct of the crosslinking reaction between humins, primarily occurs when the maximum temperature of 100 °C is reached. Although the water signal decreases afterwards, it is assumed that water is continuously released in small amounts as long as the humins are heated. This is confirmed by the significant drop in water signal intensity after the 5-hour heating step, whereas the signal does not change for fragments that were not detected throughout the experiment, therefore separating baseline and sample effects. The release of HMF increases up to 2 hours after the start of the experiment and stabilizes afterwards. The stable signal is related to continuous evaporation of HMF molecules and is in agreement with the results of the FT-IR experiment.

To verify the potential presence of other species, a control experiment was performed that included an additional scan ranging from 50 – 150 m/z (see Supplementary Information). While similar behavior could be observed for water and HMF fragments,

the release of a third compound, chlorsulfuron, was identified via fragments with m/z = 140, 111 and 69. Therefore, it is hypothesized that humins were contaminated with carbon-bound chlorsulfuron residue [43].

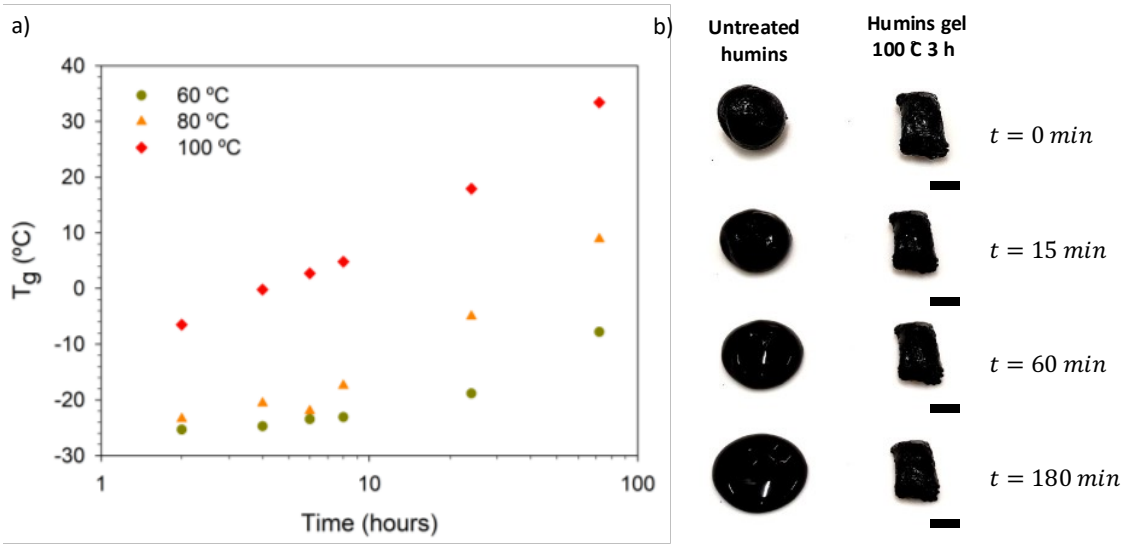

Figure 3. T_g values of humins treated at 60 ˚C (dark yellow circles), 80 ˚C (orange triangles) and 100 ˚C (red diamonds) for different timescales ranging from 2 hours to 72 hours. The results were determined using DSC during a cooling step down to −80 °C. b) Photographs of untreated humins and humins treated at 100 ˚C for 3 hours showing their shape evolution as a function of time. It can be observed that untreated humins start to slowly flow due to their viscous nature, whereas treated humins possess gel features. Scale bar: 0.5 cm

Humins are able to crosslink when heated. These crosslinking reactions are translated into a growth in M_w, which directly influences T_g. **Figure 3** displays the variations of T_g when humins were treated at 60 ˚C, 80 ˚C and 100 ˚C at different timescales ranging from 2 hours to 72 hours. Our previous studies determined the T_g of raw humins of the same nature as the ones used in this study at –26 ˚C. At 60 ˚C, only a minor increase in T_g is observed for humins even when heated for long timescales, experiencing a growth of 18 ˚C after the whole heating process. A faster T_g growth is observed when humins are treated at 80 ˚C (an increase of 35 ˚C) and 100 ˚C (an increase of 59 ˚C). At low timescales, no significant variations are observed when comparing the curing process at 60 ˚C and 80 ˚C, and only start to deviate at times above 8 hours. A different behavior is observed for the curing process at 100 ˚C, showing a more rapid increase even at low timescales. Based on previous TGA results, this can result from the combination between enhanced reaction kinetics and evaporation of humins volatile components. These rate differences are mainly observed at low curing timescales, whereas at times above 24 hours the growth rate at each temperature goes parallel with respect to each other. These trends are suggested to happen as a consequence of the evaporation of volatiles at low curing timescales, being this evaporation proportionally faster with temperature. Upon the release of volatiles, the growth in T_g is merely due to the formation of covalent crosslinks.

The photographs showed in Figure 3b show the effect of the crosslinking of humins on their macroscopic stability. It is evidenced that, while untreated humins tend to flow due to their viscous nature, humins treated at 100 ˚C for 3 hours keep their shape for prolonged times. Since T_g is still very low ($T_g < 0\ ^{\circ}C$) to yield a glass structure, it can be affirmed that humins undergo a thermal gelation process before reaching a glass state. Covalent crosslinks and supramolecular interactions (*i.e.* hydrogen bonds) can take part of the gelation process since these two are present in humins as previously observed in Figure 1. Rheology is known to be a powerful technique to assess gelation processes since the viscoelastic properties of gelling systems diverge at the gel transition [44]. Thus, a series of rheological experiments were performed to elucidate the gelation mechanism of humins, including the nature of the crosslinks forming the network.

3.2 Rheological Response of Humins at Different Temperatures

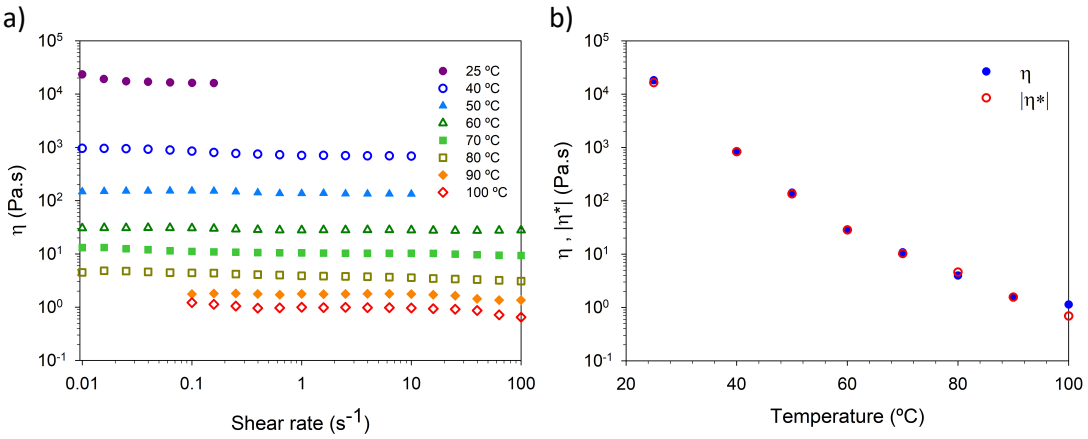

Figure 4. a) Temperature-dependence of the steady shear viscosity of humins over a temperature range of 25 – 100 ˚C. Apparent shear rates ranging from 0.01 s^{-1} to 100 s^{-1} are used except for the conditions where the response violates the instrument torque limitations. b) Relationship between the average steady shear viscosity and the average magnitude of the complex (oscillatory) viscosity over a temperature range of 25 – 100 ˚C, showing the response of a Cox-Merz material. Shear rates in the range of 0.01 – 100 s^{-1} and oscillatory frequencies in the range of 0.1 – 100 Hz were used to determine the steady shear viscosity and magnitude of the complex viscosity, respectively.

Humins are highly viscous liquids due to the large M_w of some oligomers present in their polydisperse structure that strongly influences their viscosity. The viscous response of humins in the liquid state, that is, before starting the gelation process, has been investigated in this research using both shear and dynamic rheology. **Figure 4a** shows different flow sweeps on humins submitted to different temperatures ranging from 25 ˚C to 100 ˚C. For the investigated shear rates, the steady shear viscosity (η) profiles are strongly linear, that is, they exhibit a Newtonian fluid behavior. A deviation of < 50% is observed over the evaluated shear rates. The humins also demonstrate a net decrease of nearly five orders of magnitude in η from 25 ˚C to 100 ˚C. This viscosity distribution varies linearly with the reciprocal temperature according to the Arrhenius law (see Supplementary Information). Even increasing the temperature by mild values (*i.e.* 40 ˚C or 50 ˚C), leads to a considerable decrease in their viscosity (*i.e.* from 18168 $\pm$ 2601 Pa·s

at 25 ˚C to 844 ± 106 Pa·s at 40 ˚C or 141 ± 8 Pa·s at 50 ˚C). This is interesting since humins can be thought of as either a concentrated polymer solution or a colloidal suspension based on their microstructure, which is strong shear thinning by their preparation pathway [45]. Both materials are known to present strongly non-linear rheological behaviors at elevated shear rates [46-49]. For the analyzed batch of humins, a possible explanation for the observed behavior is that humins are in the form of a soft particulate system formed by low M_w oligomeric molecules. The lack of microstructure or chain entanglements at low conversions makes temperature the only factor that influences viscosity. Similar responses were observed for other concentrated sugar-based highly concentrated solutions until they form a glass [50, 51].

To expand these observations, capillary rheometry can be an interesting tool to assess the response of humins at higher shear rates. Mechanical break-up of physical interactions that build the humins structure, shifting towards a shear-thinning response, is of great interest for prevent their polymerization upon processing under mild conditions.

The modulus of the complex viscosity (η^*) can differ from the steady shear viscosity for many complex materials due to their dependence of the shear rate and the oscillatory frequency, respectively. Cox and Merz [52] empirically confirmed this distinction for some materials, whereas other systems (regularly polymeric liquids referred to as "Cox–Merz materials") present the same values under both shear and oscillation. **Figure 4b** shows how the viscosity of humins behaves under the mentioned deformation conditions. Interestingly, humins hold to the Cox-Merz rule, displaying a full agreement between steady shear and linear viscoelastic values, only modestly differing at 100 ˚C. However, viscosities measured at 100 ˚C might yield less reliable experimental results due to the occurrence of crosslinking reactions during the measurement. The measurement timescales were similar to account for this issue, so the observed mismatch is proposed to be the result of flow-enhanced reaction kinetics by facilitating the contact between reacting species or simply due to inertial effects measuring at high frequencies.

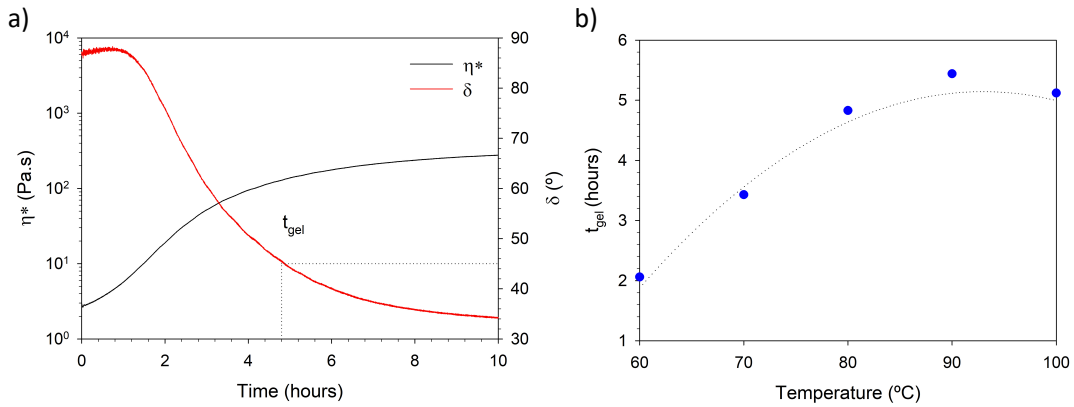

Figure 5. a) Magnitude of the complex viscosity ($|\eta^*|$) and phase angle (δ) as a function of time when heated at 80 ˚C. The gelation time (t_{gel}) is observed after 4.83 hours as the point where δ = 45˚, that is, G' = G". b) t_{gel} values determined at different temperatures. The obtained t_{gel} (in hours) is 2.04, 3.43, 4.84, 5.43 and 5.10 for a

temperature of 60 ˚C, 70 ˚C, 80 ˚C, 90 ˚C and 100 ˚C, respectively. An oscillatory strain (γ) of 0.1% and an oscillatory frequency of 1 Hz were used during the experiment.

A generalized method for the determination of the gel point relies on the crossover point of G' and $G"$ as a function of time under oscillation at a constant frequency. Small amplitude oscillatory shear (SAOS) tests have the advantage to continuously monitor the gelation process averting the disruption of the evolving microstructure[44]. **Figure 5a** shows an example of the isothermal evolution of the viscoelastic properties of humins during their crosslinking process. In this example, the temperature is kept at 80 ˚C during the entire experiment. At early polymerization stages, that is, low reaction times, a viscous behavior clearly dominates, with a phase angle close to 90˚. Low dynamic viscosity values are also observed, coinciding with the value previously observed in **Figure 4b**. As time goes on, a decrease in δ is observed as a consequence of humins crosslinking reactions, being G' growth more pronounced than $G"$. The process evolves until a $G'/G"$ intersection (phase angle of 45˚) is reached, which is set as the material gel point. At this point, a percolated molecular structure is accomplished so that the elastic behavior becomes predominant. As the reaction continues, humins gels behave as solid viscoelastic materials with continuously growing viscoelastic properties. During the studied temperatures and timescales, the full conversion of humins is still far from being reached, hence the use of higher temperatures or a catalyst are needed for this purpose[38]. At this temperature, eventually a reduction in the viscoelastic parameters slope is observed due to the retarded reaction kinetics upon percolation of the network. The same experiment was performed at different temperatures (from 60 ˚C to 100 ˚C at 10 ˚C intervals) to assess the influence of the reaction temperature on the gelation kinetics. **Figure 5b** counterintuitively shows a delay in gelation at higher temperatures. This is in contrast with conventional step-growth polymerization reactions that are regularly favored at elevated temperatures. Considering the proposed polymerization mechanisms of humins, dominating aldol addition and condensation but also etherification, esterification or acetalizations, it is reasonable to expect that humins would hold a similar response. In addition, a maximum t_{gel} is reached at 90 ˚C, slightly decreasing at 100 ˚C.

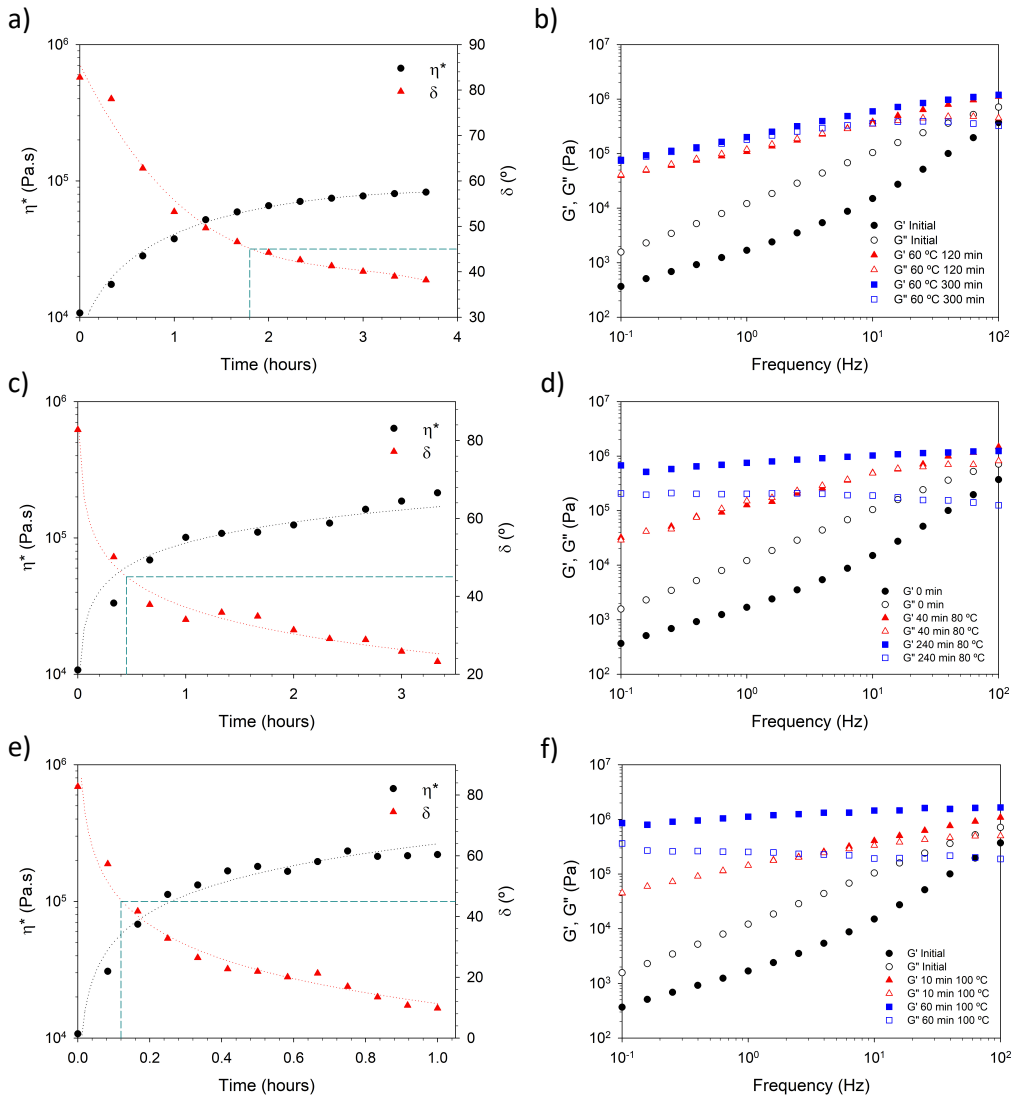

Figure 6. a) $|\eta^*|$ and δ development of humins as a function of time when heated up stepwise. Each point is taken at room temperature after a thermal treatment at 60 ˚C for 20 minutes. t_{gel} is observed after 1.83 hours of experiment as indicated by the blue dashed line. b) G' and $G"$ as a function of the oscillatory frequency for humins at different stages of their polymerization (initial, as a critical gel and beyond t_{gel}) reacted at 60 ˚C. The same process is repeated for a reaction temperature of c) d) 80 ˚C and e) f) 100 ˚C, observing t_{gel} values of 43 minutes and 10 minutes (in this case, each point is taken at room temperature after a thermal treatment at 100 ˚C for 5 minutes), respectively.

To avoid any influence of temperature on the viscoelastic response of humins during the gelation process, stepwise gelation experiments were performed. These stepwise gelation experiments consist on the pre-conditioning of humins at a certain temperature (*e.g.* 60 ˚C, 80 ˚C and 100 ˚C) to let them react, followed by their equilibration at room temperature prior measuring of the viscoelastic response. This allows the rheological properties of humins to be measured in a steady state throughout the whole polymerization process. Thus, not only the gelation process can be monitored but also hinders the possibility to disrupt any thermoreversible physical interactions intervening

in the formation of the gel structure. In contrast with **Figure 5**, **Figure 6** shows how an increase in temperature leads to enhanced gelation kinetics. All the measured viscoelastic parameters display a power law behavior as previously observed for isothermal experiments but growing faster at higher temperatures and low timescales. The main difference between the studied temperatures is observed at the gel point. Gelation at 60 ˚C leads to a very close t_{gel} than under isothermal conditions, that is, 1.83 hours, whereas at 80 ˚C and 100 ˚C the determined gel points are shown at 43 min and 10 min, respectively. The obtained results are in line with the expected behavior of step-growth polymerization processes. In addition, G' of the samples cured at higher temperatures increases at a higher rate, yielding a higher plateau value beyond the gel point. This is translated into a higher crosslink density, turning into a higher elastic response. There is also a clear difference between the G' plateau value of the example shown in **Figure 5** cured at 80 ˚C and the stepwise counterpart in **Figure 6**. As can be seen, G' is much lower when humins gels are kept at 80 ˚C even beyond the gel point, so that temperature has a strong softening impact on humins gels. The same effect is observed for the dynamic viscosity, being inversely proportional to the phase angle.

Frequency sweeps were performed to further examine structural changes of humins at different stages of polymerization (**Figure 6**). For raw humins below the gel point, it is revealed a viscous behavior presenting $G"$ > G' (or $\tan(\delta)$ > 1). In the low frequency region, it is observed a $G'(\omega)$ and $G"(\omega)$ relationship of: $G' \approx \omega^{0.67}$ and $G" \approx \omega^{0.87}$. At high frequencies, there is a pronounced deviation on the slope of $G' \approx \omega^{1.42}$. It is presumed that this deviation at high frequencies are due to inertial effects during the measurement. $G"$ remains constant all along the measured frequency range. For regular polymer solutions and melts composed of linear chains, G' and $G"$ possess apparent exponents of approximately 2 and 1, respectively. The observed deviations are expected to be caused, inter alia, to a predominant humins viscous behavior due to the poor crosslink density along with highly polydisperse and branched polymeric chains which are able to relax, providing a certain elasticity manifested in the high frequency region [53]. A time-temperature/time-cure superposition can be applied to build a master curve that incorporates both the time-temperature superposition at each temperature at different stages of the polymerization, as well as the information regarding the curing at different temperatures (i.e. 60 ˚C, 80 ˚C and 100 ˚C). This master curve can be found in the Supplementary Information, deviating just in the low-frequency region since this corresponds to the structure development of humins below the gel transition temperature.

Considering the stepwise experiments in **Figure 6**, the Arrhenius equation (**Equation 1**) allows to calculate an activation energy (E_a) of 66 kJ/mol during the gelation process (See Supplementary Information). The obtained value is in line with previous reports that calculated the activation energies of humins polymerizing below the gel point using other characterization methods[38].

$$\ln\left(t_{gel}\right) = \frac{E_a}{RT} + \ln(A) \quad (1)$$

3.3 Elucidation of the critical gel structure

The G' and $G"$ crossover is an extended criterion to indicate the gel point during a sol-gel or gel-sol transition. It is a well-established method to evaluate the gelation phenomena due to its simplicity. However, it presents the inconvenience of the dependence of G' and $G"$ on frequency. To this end, according to the Winter and Chambon criteria, the gel point can be accurately defined as the point where $G'(\omega)$ and $G'(\omega)$ show a power law dependence on the oscillation frequency[54-56]:

$$G'(\omega) \sim G"(\omega) \sim \omega^n \quad 0 < n < 1 \; at \; the \; gel \; point \tag{2}$$

and the loss angle becomes independent of frequency:

$$tan\delta = \frac{G"}{G'} = tan\frac{n\pi}{2} \tag{3}$$

where n is the critical relaxation exponent. The n value can provide insightful information about the molecular structure of the system during the gelation process. For many gels following this approach, $G' = G"$ at the gel point and thus n = 0.5. This is valid for polymers growing in a flexible linear fashion rather than an irregular branched approach. However, there exist critical gels that do not follow this behavior, so n can deviate from this value. Small n values (0 < n < 0.5) correspond to stiff and strong gels whereas large *n* values (0.5 < n < 1) represent soft and weak gels[57].

Conditioning humins at 60 ˚C, 80 ˚C and 100 ˚C during their corresponding gelation times develops into the typical rheological response of a critical gel. This is translated into parallel viscoelastic moduli and a frequency independent loss angle as previously described in **Equation 2** and **Equation 3**. As illustrated in **Figure 6**, G' and $G"$ overlay over a wide frequency range at the gel point, deviating at high frequencies by decreasing $G"$ (or a decrease in the loss angle). The superimposed viscoelastic moduli at 1 Hz means that the previous isofrequency gelation experiments shown in **Figure 5 and Figure 6** pertain to the most dominant range of experimental frequencies. At this point, for the studied reaction temperatures, it is determined a critical relaxation exponent $n \approx 0.5$. This value matches other observations for stoichiometrically balanced gels based on linear flexible polymer chains such as PDMS and polyurethane[55, 56]. This would indicate that humins tend to grow by crosslinking in a compact, linear polymeric fashion rather than highly branched (n > 0.5) under the investigated conditions. However, this is in contrast with the expected growth behavior of humins considering their multifunctional and irregular chemical structure. At longer reaction times, the results exhibit a clear viscoelastic solid behavior (G' > $G"$ or $tan\delta$ < 1). This difference is barely visible at 60 ˚C even letting humins react for 300 min, behaving as a critical gel over the entire frequency range. This is ascribed to the low reaction conversions reached after the creation of a connected microstructure at such low temperatures, hindering the reactants mobility to continue the growth of humins. By curing at higher temperatures and long timescales, that is, 80 ˚C and 100 ˚C, a clear G' plateau is reached along the entire accessible frequency range. Further investigation is needed to understand how humins form a gel

under different conditions such as under the presence of Brönsted acids or using humins from different polysaccharides feedstocks.

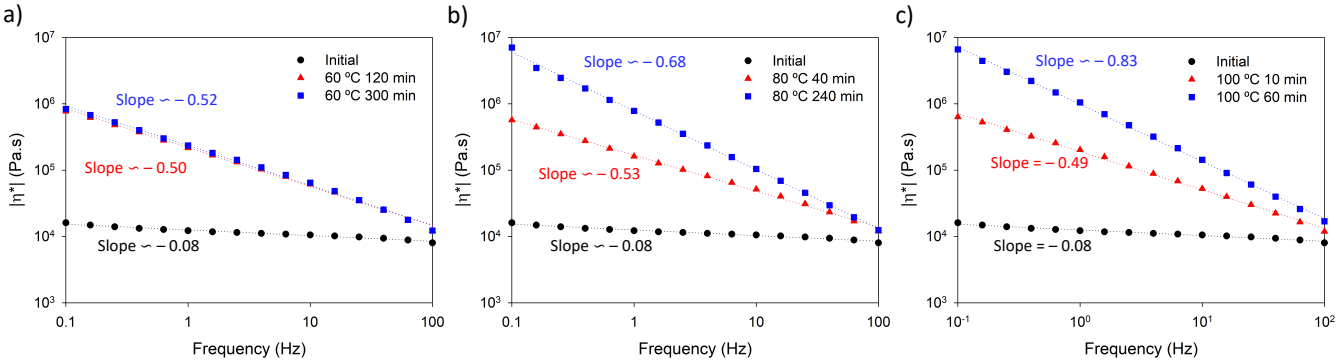

Figure 7. $|\eta^*|\,(\omega)$ for humins at different stages of their polymerization (initial, as a critical gel and beyond t_{gel}) reacted at a) 60 ˚C, b) 80 ˚C and c) 100 ˚C.

The modulus of the complex viscosity is another viscoelastic parameter strongly influenced by the analysis frequency and can bring useful information about the gelation process. The M_w of the growing humins clusters diverges at the gel point, hence the same behavior is observed for η^* as a consequence of the remarkable change in elasticity upon percolation. Its dependence of the frequency is also related to the critical relaxation exponent as expressed in the following equation[58]:

$$\eta^*(\omega) \sim \omega^{n-1} \tag{4}$$

The changes in η^* with frequency at different polymerization stages are displayed in **Figure 7**. Initially, η^* of humins behaves independent of the frequency according to their Newtonian liquid behavior. By increasing the gelation times up to the gel point, a clear shear-thinning behavior is observed for all frequencies with a curve slope of ≈ -0.5 ($n \approx 0.5$) for all the reaction temperatures. These results align with the results reported in **Figure 6** for humins critical gels. As previously observed, the reaction at 60 ˚C does not evolve further at longer timescales and remains in a state close to a critical gel. Higher temperatures develop the degree of polymerization of humins, reaching higher zero-shear viscosity values and a more pronounced shear-thinning behavior (steeper slopes). Considering the molecular nature of humins, this is in agreement with the theory of the presence of both supramolecular and covalent interactions in humins gels. Physical interactions are reversible not only by heating but also applying external mechanical forces, leading to a pronounced shear-thinning response that can even lead to the gel yielding. Newtonian behavior is observed for unreacted humins with poorly concentrated high M_w polymer chains that can undergo percolation by physical crosslinks. A growth in the size of humins leads to the percolation of clusters by both chemical and physical interactions, strongly influencing the subsequent gel elasticity. The application of shear forces to a humins critical gel impedes humins to withstand the gel network yielding the physical interactions. At long timescales where chemical bonds are dominant, humins are crosslinked by irreversible and strong covalent bonds, exhibiting a glassy behavior that leads to a non-recoverable fractured state upon yielding.

There is no universal value for n since it can deviate even for the same system by forming gels tuning different gelation parameters. Aspects such as the aging process kinetics, use of catalysts, polymer concentration, molecular weight, defects in the gel network or the pre-gel history make n a complex parameter to assess the behavior at the gel point[57, 59]. The non-linear parameter n can be related to the critical gel network structure by means of the fractal scaling concept. Generally, fractal objects are composed of a range of self-similar structures of different length scales. It is known that gelation processes lead to the formation of relatable fractal structures, and their self-similar structure can be quantified by the fractal dimension (d_f). As shown in **Equation 5**, d_f is related to the molecular weight of a polymeric cluster, M_w, and the radius of gyration, R, as:

$$R \approx M_w^{1/d_f} \tag{5}$$

The fractal dimension at the gel point is commonly defined for crosslinked gels by the percolation cluster at threshold theory. This is based on the divergence of the viscosity at the gel point, which is caused by the formation of a self-similar fractal structure with infinite molecular weight[60]. By screening out the excluded volume effect (two monomers cannot coincide at the same place) and the intramolecular and intermolecular hydrodynamic interactions, Muthukumar *et al.*[61] related n to the fractal dimension using the following expression:

$$n = \frac{d(d+2-2d_f)}{2(d+2-d_f)} \tag{6}$$

where d is the space dimension (for our three-dimensional case, d = 3). As a general principle, large d_f values reflect more uncondensed and irregular gel structures, and vice versa[57]. Using **Equation 6**, a d_f value of 2.00, 1.96 and 2.01 are calculated for humins critical gels when gelled at 60 ˚C, 80 ˚C and 100 ˚C, respectively. The results obtained are in agreement with a reaction-limited cluster aggregation (RLCA) process (d_f^{RLCA} = 1.9 – 2.1) and not with a diffusion-limited cluster aggregation (DLCA) process (d_f^{DLCA} = 1.7 – 1.8)[62]. It is observed that the curing temperature does not influence the fractal gel morphology of humins self-similar gels. Considering the chemical structure of humins, the percolation theory finds d_f = 2.52 for self-similar branched polymers, not matching the previous observations. However, these values can be shifted to lower ones depending on discrepancies on the polymer state such as solvent swelling or polydispersity[63]. Previous fractal studies on polymer gels proved that, for $d_f \approx 2$, it can be inferred that polydispersity can strongly affect the final fractal structure and thus the final network mechanical properties. Lairez *et al.*[64] assessed the percolation theory of model branched polyurethane systems observing similar d_f values as the ones obtained for humins. However, they verified that, correcting the clusters mass distribution, polydisperse branched polyurethanes in a native polymer form (*i.e.* no solvent swelling influence) displayed a d_f = 2.50, matching the percolation theory. Based on the branched and the multitude of reactive functional groups in the structure of identified humins intermediates, a similar behavior can be expected. This hypothesis agrees with the results reported by Cheng *et al.*[39] who observed the formation of polydisperse fractal-like structures upon humins condensation and aggregation via x-ray scattering.

3.4 Gel Formation Mechanism

It is clear that temperature plays a major role in the gelation process of humins. As observed in both the isothermal and the stepwise experiments, different gel points are obtained by just modifying the thermal history during the rheological analysis. The dependence of the viscoelastic properties of conventional gels with temperature can be explained considering the nature of the crosslinks forming the network. For chemical gels interconnected by permanent covalent bonds, the viscoelastic properties are barely influenced by temperature, experiencing a substantial modification of their properties only when heated or cooled above T_g. These networks can be fragmented only when thermoreversible covalent bonds (*i.e.* Diels-Alder bonds[65, 66]) are present in their structure. On the other hand, supramolecular gels (also referred to as transient networks) are crosslinked by transient physicochemical interactions (*i.e.* hydrogen bonds or electrostatically-driven associations[67]). These weak bonds are able to form solid gels but are reversible under external energetic stimuli such as temperature or mechanical forces, entailing dramatic changes in the material viscoelastic properties[68, 69]. Also, these bonds are reversible, that is, a fragmented gel can be reformed and recover its mechanical properties and functionality.

Based on the observed results and existing studies on humins' chemical structure and aggregation dynamics, we hypothesize that humins gels are structured under a trade-off between the degree of physical and chemical crosslinks. An increase in temperature triggers both humins crosslinking processes and the dissociation of weak physical interactions. At low polymerization stages, that is, low reaction temperatures or timescale, the rheological behavior of humins is governed by associative physical interactions[17]. This includes functional groups that can create hydrogen bonds such as hydroxyl or carbonyl groups present in humins structure[10-12, 40] or interactions between soluble molecules adsorbed on humins hydrophobic solid surfaces[39, 41]. However, at this point of the polymerization reaction, the deficient M_w of humins is not high enough to form a solid gel even under the presence of abundant physicochemical interactions. This can be confirmed observing the response of the viscosity of humins increasing the temperature, so that the thermal dissociation of these interactions drastically reduces the viscosity even under mild heating conditions as observed in **Figure 4**.

As the reaction proceeds, new chemical crosslinks are formed and humins continue growing in M_w. At a given reaction extent, humins yield enough covalent crosslinks to withstand a solid state even at elevated temperatures. However, the resulting gel is structured by a combination of the newly created covalent bonds and the previously existing physical interactions, which are more abundant at low temperatures. Thus, by thermally neglecting the influence of supramolecular interactions on the structure gel of humins, a delay in the gel formation is expected as the temperature increases. This is proven in the isothermal experiments exhibited in **Figure 5,** showing a delay in gelation as the temperature increases, where the concentration of physical bonds is substantially reduced. As an exception, at 100 ˚C the gel forms faster than at 90 ˚C, so it is considered that, under these conditions, the reaction kinetics are substantially favored and can compensate the loss of physical interactions.

The stepwise experiments show the formation of a gel when humins are measured at room temperature instead of at elevated temperatures over the course of the rheological analysis. The main difference compared to isothermal experiments resides on the viscoelastic properties of humins, which are also influenced by the physical interactions lost during heating. Comparing the isothermal gelation results (**Figure 5**) and the stepwise gelation experiments (**Figure 6**), there is an evident shift to lower gelation times as the temperature increases in stepwise experiments, opposed to the isothermal measurements. This results from the influence of the additional interactions which were previously neglected in the isothermal experiments, being now actively involved in the formation of a gel. This leads to faster gelation times, increasing the gelation rate at higher polymerization temperatures (as previously shown in **Figure 6**). Based on the obtained results, it is stated that the formation of new covalent crosslinks allows humins to further grow as an intermediate physicochemical gel formed by bigger humins clusters able to percolate by physical crosslinks. As previously described, further crosslinking eventually shifts humins towards a gel governed by chemical bonds, ultimately taking the main role of its viscoelastic properties and lessening the relevance of the remaining physical interactions. Thus, the control of humins degree of covalent crosslinking allows to tailor the resulting gel properties, moving from a transient network to a covalent network. This whole process is schematized in **Figure 8**. This is of great interest for humins, especially when their application aims for their valorization as materials since their degree of crosslinking is going to strongly influence the resulting rheological and mechanical properties. Thus, choosing a suitable rheological characterization protocol is essential to understand the growth of humins to optimize their processing conditions.

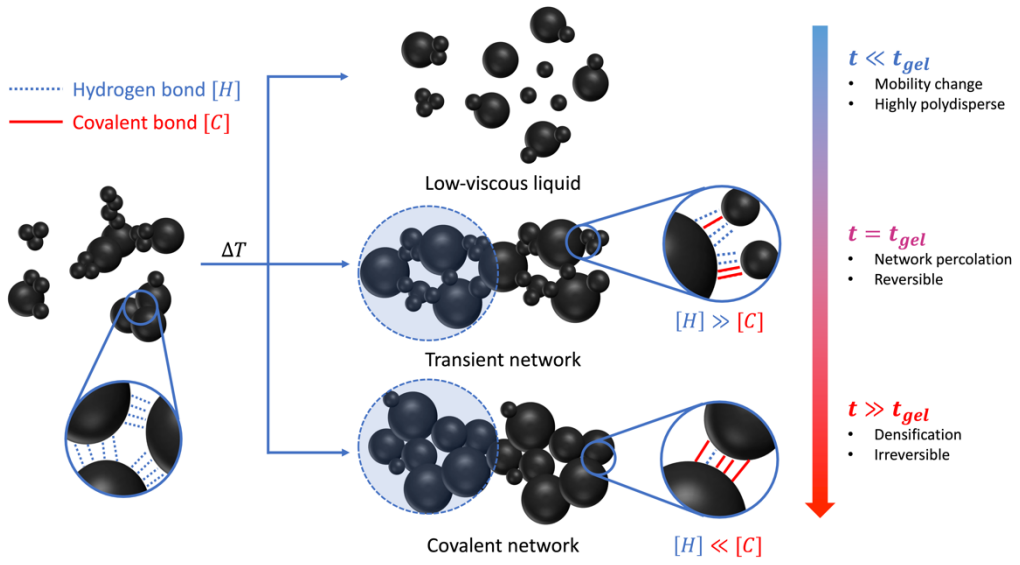

Figure 8. Schematic representation of humins gelation process. Initially, humins are present as a polydisperse soft particulate liquid system yielding high viscosity values at room temperature due to the presence of abundant hydrogen bonds. By increasing the temperatures, at short timescales ($t \ll t_{gel}$), these reversible bonds are cleaved, thus turning humins into a low-viscous liquid. Sustained elevated temperatures timescales lead to the crosslink and growth of humins particles, eventually reaching a percolated

gel state ($t = t_{gel}$). This gel is crosslinked by a mixture of both hydrogen and covalent bonds, being hydrogen bonds prevalent thus enabling gel reversibility (thermally or mechanically). Longer thermal treatments lead to the formation of a denser gel with higher thermal stability due to the formation of new covalent crosslinks. This eventually leads to the formation of an irreversible covalent network when holding elevated temperatures at $t \gg t_{gel}$. The blue circles on the gel structures indicate the self-similar fractal structures formed upon gelation.

3.5 Reverse Gelation of Humins

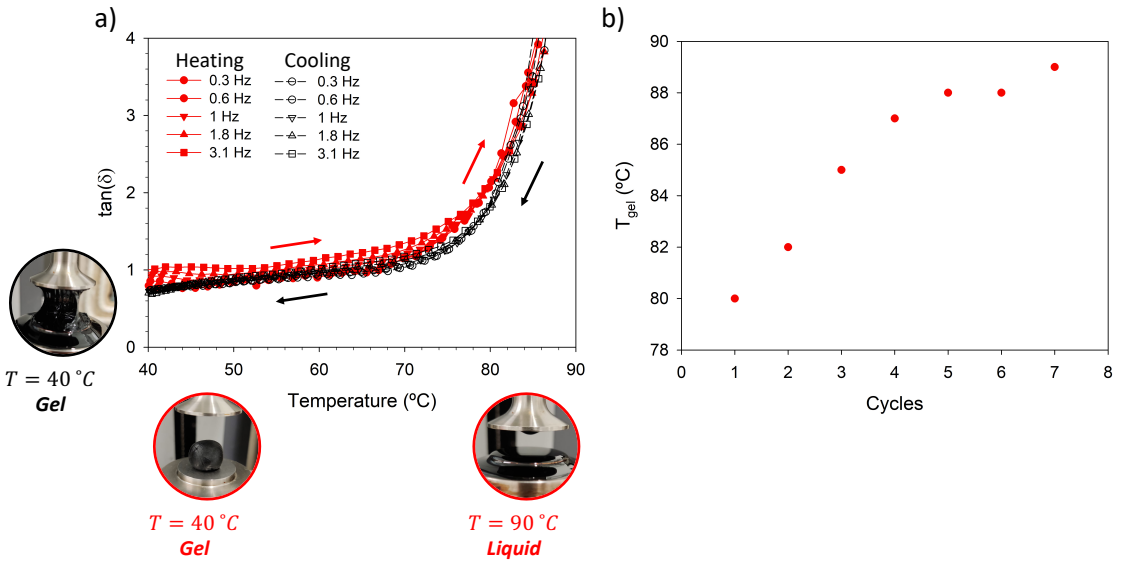

Figure 9. a) Degelation experiments on pre-heated Humins consisting on multi-frequency oscillatory heating and cooling ramps at a heating/cooling rate of 2 ˚C/min from 25 ˚C to 100 ˚C. Humins were cured for 300 min at 80 ˚C and stabilized at 25 ˚C for 1 hour before the start of the experiment (bottom picture with red edge). The gel point is determined as the point where $\tan(\omega)$ becomes frequency independent (in this case, $T_{gel} \approx 80$ ˚C). Above T_{gel}, a low-viscous liquid is obtained (right picture with red edge), which is reversibly turned into a solid gel by cooling below T_{gel} (left picture with black edge). b) T_{gel} determination after seven heating-cooling cycles, staying isothermally at 100 ˚C for 5 min at the end of each heating cycle and subsequently cooling.

A remarkable characteristic of transient networks is their ability to undergo reverse gelation at temperatures above T_{gel}. Deformation forces or temperature can provide sufficient energy to break these bonds, eventually reaching a flowing state lacking any interconnected microstructure[70]. Humins, as a physical gel, are prone to undergo this transition, not exclusively under flow (developing a yield stress) but also when exposed to elevated temperatures. For this purpose, humins that were previously reacted at 80 ˚C for 300 min were then submitted to a temperature ramp of 2 ˚C/min and corresponding viscoelastic response was measured. The results, available in **Figure 9a**, confirm this hypothesis. It is shown that, during the experiment, at a temperature of 80 ˚C the $\tan(\omega)$ values measured at different frequencies converge, that is, humins viscoelastic response becomes independent of the measurement frequency. This

corresponds to the definition of the gel point. Subsequently, cooling degelled humins leads to a decrease in $\tan(\omega)$, reaching another gel point that nicely coincides with T_{gel} measured upon heating. This proves the thermal reversibility of humins gels, confirming the physically-crosslinked nature of humins gels. In addition, the loss angle values at the gel point under both heating and cooling differ from the values exhibited in **Figure 6**, that is, $\tan(\omega) \neq 1$. A possible explanation is the alteration of the gel structure under thermal disruption due to the dynamic formation and deformation of physical crosslinks, differing from the quiescent gel structure.

Furthermore, **Figure 9b** demonstrate that the presence of irreversible covalent crosslinks shifts this solid-to-liquid transition towards higher temperatures. An isothermal conditioning of humins at 100 ˚C for 5 min at the end of each heating ramp yields humins to further polymerize. This increases the amount of irreversible bonds forming the network structure. Performing several heating-cooling cycles turns into a growth in T_{gel}, stabilizing around at 90 ˚C under the proposed conditions. Variations in the T_{gel} growth rate can be strongly influenced modifying reaction parameters such as the reaction time, temperature or the presence of an acid catalyst as it occurs with T_g[38]. Humins' valorization greatly improves the circularity of many biorefinery processes by reducing waste formation. However, chemical crosslinking of humins can be detrimental for the circularity of humins-based materials. The thermal reprocessability of these materials is crucial in case they lose their working lifespan, and eventually hindered as the M_w of humins grow. However, the use of humins as a physical gel allows these materials to be reprocessed under mild thermal conditions that can minorly influence their mechanical properties if properly designed[29, 71]. This can apply for a limited number of reprocessing cycles that will be influenced by the processing conditions, which in turn also reinforces the reprocessed materials due to the growth of stiff humins clusters.

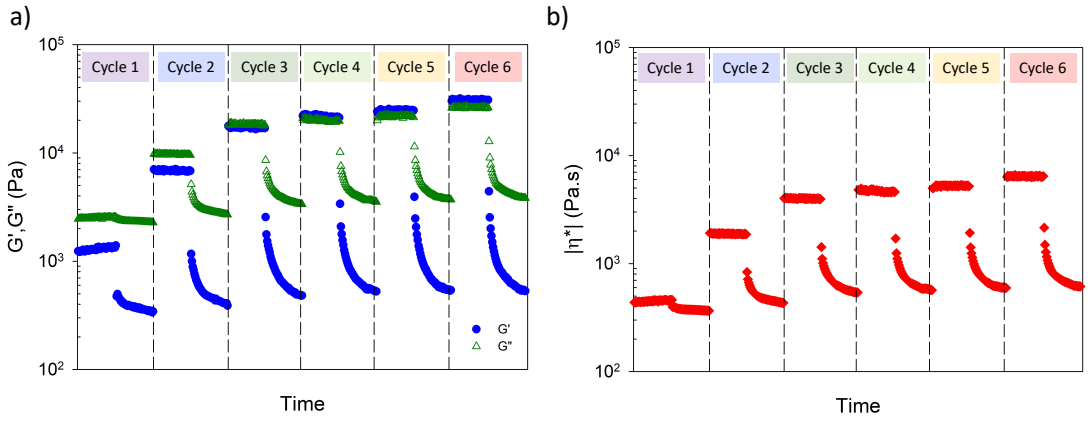

Figure 10. Dynamic rheological measurements at 50 ˚C showing the reversibility of humins gels. Initially, a low strain amplitude of 0.1 % is applied to humins to show their steady viscoelastic behaviour, whereas a larger strain amplitude of 10 % is applied to break the physical interactions forming the structure of humins. After each deformation cycle, humins were cured at 100 ˚C for 10 minutes and cooled back to 50 ˚C, equilibrating at this temperature for 10 minutes before the start of the next cycle. The cyclic loading experiments display the reversibility of humins as a function of a) G' and $G"$, and b) $|\eta^*|$.

The reversibility on physical gels can also be characterized under shear. After shear rejuvenation under large strain amplitudes, physical gels are able to restructure and restore their viscoelastic properties upon cessation of non-linear deformation[72]. In contrast to physical gels, chemical gels cannot restore mechanically cleaved crosslinks, remaining as a liquid-like system rather than an interconnected gel network. Humins gels rejuvenation and reformation at 50 ˚C are shown in **Figure 10**. A temperature of 50 ˚C is chosen to lower the viscosity of humins enough to be submitted to a large strain amplitude of 10% while preventing humins chemical crosslinking. Six different cycles are displayed. after each cycle, humins were cured at 100 ˚C for 10 minutes, being subsequently cooled back to 50 ˚C and equilibrated for other 10 minutes prior starting the next cycle. This method allows not only to recover the broken physical interactions of the network but also to create new covalent crosslinks that eventually allow the gelation of humins. **Figure 10a** clearly shows the reversibility of humins and the influence of curing on G' and $G"$. The gel point is delayed. compared to the one showed in **Figure 6** due to the physical interactions lost at a temperature of 50 ˚C. A gel network is formed between cycles 3 and 4, being $G' > G"$. This gel structure collapses at large deformations, being subsequently restored when mechanical perturbations are removed. A similar behavior can be observed for η^* in **Figure 10b**, showing a clear shear thinning behavior at large deformations, whereas low deformations show a steady response with greater η^* magnitudes as the chemical crosslinking process progresses.

4. Conclusions

The thermal gelation process of humins was investigated in this study, focusing on rheological experiments. The presence of abundant hydrogen bonds was confirmed using FT-IR spectroscopy. These hydrogen bonds are thermally unstable and led to a drastic decrease of the viscosity of humins even under mild thermal conditions. However, exposing humins to high temperatures also triggers their polymerization, continuously growing their M_w. This was confirmed by a growth in T_g of humins when submitted to temperatures above 60 ˚C, even without the need of a Brönsted acid catalyst. At a certain stage of polymerization, dynamic rheology confirmed the formation of a percolated gel, and the gel formation is delayed by staying isothermal during the gelation process as a consequence of losing hydrogen bonds. Performing gelation experiments stepwise turned into the formation of a gel in line with conventional step-growth polymerization processes. Thus, the combination of supramolecular and covalent crosslinks plays an important role in the final humins gel structure, shifting from a physical to a chemical gel as the polymerization process continues. This characteristic rheological behavior of humins has been previously observed in other systems such as proteins[73, 74] or interpenetrated polymer networks[75, 76], which are crosslinked by both supramolecular (*e.g.,* hydrogen bonds, ionic or metal-ligand interactions) and dynamic covalent bonds (*e.g.,* disulfide or Schiff-base bonds).

The critical gel structure is strongly influenced by the polydispersity of humins, sharing features with other polydisperse gels available in literature. A fractal dimension $d_f \approx 2$ confirms that the gelation of humins evolves through a RLCA process rather than a DLCA process for all the studied conditions. In addition, due to the presence of an important concentration of physicochemical interactions even in the gel state, humins gels are able

to undergo reversible gelation process when heated up. Longer periods at elevated temperatures shift the gelation temperature towards higher temperatures due to the continuous formation of irreversible chemical crosslinks. These results are essential to understand the behavior of humins under typical processing conditions, and the final gel state will influence some material features such as the mechanical properties or reprocessability. These results are presented as a toolbox for researchers to analyze the rheological evolution of different batches of humins during polymerization, aiming to optimize the final material properties and ensure reproducibility. Using the proposed methods to synthesize new humins-based materials, as well as study the influence of other parameters on humins gels (*i.e.* the presence of a catalyst, use of humins derived from different feedstocks…), are interesting research lines to assess the potential of humins as a replacement for fossil-based resources. Aging of humins can also influence the studied properties by *e.g*. slow evaporation of volatile molecules or residual crosslinking reactions under mild conditions in the long term during, for example, their shelf-life. Similarly, oxidation of humins under the presence of external agents (*e.g.* UV-light, contaminants…) can also affect their rheological properties. The modification of oxidable functional groups, thus changing the nature of the present supramolecular interactions, or the fractionation of humins by cleaving ether moieties present in the humins structure[10], will lead to changes in their thermorheological response. These aspects are still poorly understood yet having a detrimental impact on the stability of humins and their behaviour.

Acknowledgements

The authors gladly acknowledge Avantium Renewable Chemicals BV for providing the humins used for this research and the Research Foundation Flanders (FWO-Vlaanderen) for financially supporting the FWO Project AMSeR (G028218N) and the FWO fellowship 1SA7320N of Giel Arnauts.

References

1. P. Anastas and N. Eghbali, *Chemical Society Reviews*, 2010, **39**, 301-312.
2. C. Lin, A. Koutinas, K. Stamatelatou, E. Mubofu, A. Matharu, N. Kopsahelis, L. Pfaltzgraff, J. Clark, S. Papanikolaou, T. Kwan and R. Luque, *Biofuels Bioproducts & Biorefining-Biofpr*, 2014, **8**, 686-715.
3. E. de Jong, H. R. A. Visser, A. Sousa Dias, C. Harvey and G.-J. M. Gruter, *Polymers*, 2022, **14**, 943.
4. G. Yang, E. Pidko and E. Hensen, *Journal of Catalysis*, 2012, **295**, 122-132.
5. L. Mika, E. Csefalvay and A. Nemeth, *Chemical Reviews*, 2018, **118**, 505-613.
6. S. Kang, J. Fu and G. Zhang, *Renewable & Sustainable Energy Reviews*, 2018, **94**, 340-362.
7. P. Sudarsanam, E. Peeters, E. Makshina, V. Parvulescu and B. Sels, *Chemical Society Reviews*, 2019, **48**, 2366-2421.
8. B. Velaga, R. Parde, J. Soni and N. Peela, *Microporous and Mesoporous Materials*, 2019, **287**, 18-28.
9. N. Ramli and N. Amin, *Applied Catalysis B-Environmental*, 2015, **163**, 487-498.

10. I. van Zandvoort, Y. Wang, C. Rasrendra, E. van Eck, P. Bruijnincx, H. Heeres and B. Weckhuysen, *Chemsuschem*, 2013, **6**, 1745-1758.
11. Z. Cheng, J. Everhart, G. Tsilomelekis, V. Nikolakis, B. Saha and D. Vlachos, *Green Chemistry*, 2018, **20**, 997-1006.
12. L. Filiciotto, A. Balu, A. Romero, C. Angelici, J. van der Waal and R. Luque, *Molecular Catalysis*, 2019, **479**, 5-16.
13. N. Shi, Q. Liu, X. He, G. Wang, N. Chen, J. Peng and L. Ma, *Energy & Fuels*, 2019, **33**, 9904-9915.
14. S. Dee and A. Bell, *Chemsuschem*, 2011, **4**, 1166-1173.
15. V. Maruani, S. Narayanin-Richenapin, E. Framery and B. Andrioletti, *Acs Sustainable Chemistry & Engineering*, 2018, **6**, 13487-13493.
16. E. Pfab, L. Filiciotto and R. Luque, *Journal of Chemical Education*, 2019, **96**, 3030-3037.
17. S. Liu, Y. Zhu, Y. Liao, H. Wang, Q. Liu, L. Ma and C. Wang, *Journal*, 2022, **10**.
18. J. Sun, H. Cheng, Y. Zhang, Y. Zhang, X. Lan, Y. Zhang, Q. Xia and D. Ding, *Journal of Energy Chemistry*, 2021, **53**, 329-339.
19. Y. Liao, S. Koelewijn, G. Van den Bossche, J. Van Aelst, S. Van den Bosch, T. Renders, K. Navare, T. Nicolai, K. Van Aelst, M. Maesen, H. Matsushima, J. Thevelein, K. Van Acker, B. Lagrain, D. Verboekend and B. Sels, *Science*, 2020, **367**, 1385-+.
20. S. Kang, J. Fu, G. Zhang, W. Zhang, H. Yin and Y. Xu, *Polymers*, 2017, **9**.
21. P. Tosi, G. van Klink, A. Celzard, V. Fierro, L. Vincent, E. de Jong and A. Mija, *Chemsuschem*, 2018, **11**, 2797-2809.
22. P. Tosi, G. van Klink, C. Hurel, C. Lomenech, A. Celzard, V. Fierro, C. Delgado-Sanchez and A. Mija, *Applied Materials Today*, 2020, **20**.
23. X. Chen, N. Guigo, A. Pizzi, N. Sbirrazzuoli, B. Li, E. Fredon and C. Gerardin, *Polymers*, 2020, **12**.
24. M. Ma, N. Liang, P. Hou, P. Zhang, J. Cao, H. Liu, X. Xu, H. Yue, G. Tian and S. Feng, *Chemistry-a European Journal*, 2021, **27**, 12659-12666.
25. C. Cantarutti, R. Dinu and A. Mija, *Biomacromolecules*, 2020, **21**, 517-533.
26. E. Licsandru, M. Gaysinski and A. Mija, *Polymers*, 2020, **12**.
27. R. Dinu, M. Gaysinski, E. De Jong and A. Mija, *Journal*, 2022, **87**.
28. R. Dinu and A. Mija, *Green Chemistry*, 2019, **21**, 6277-6289.
29. K. Cerdan, J. Brancart, E. Roels, B. Vanderborght and P. Van Puyvelde, *Polymers*, 2022, **14(9)**, 1657.
30. D. Chernysheva, Y. Chus, V. Klushin, T. Lastovina, L. Pudova, N. Smirnova, O. Kravchenko, V. Chernyshev and V. Ananikov, *Chemsuschem*, 2018, **11**, 3599-3608.
31. A. Sangregorio, N. Guigo, L. Vincent, E. de Jong and N. Sbirrazzuoli, *Polymers*, 2022, **14**.
32. G. Tzvetkov, M. Nedyalkova, J. Zaharieva, T. Spassov and B. Tsyntsarski, *Powder Technology*, 2019, **355**, 83-92.
33. L. Filiciotto, A. Balu, A. Romero, E. Rodriguez-Castellon, J. van der Waal and R. Luque, *Green Chemistry*, 2017, **19**, 4423-4434.
34. C. Lomenech, C. Hurel, L. Messina, M. Schembri, P. Tosi, F. Orange, F. Georgi, A. Mija and P. Kuzhir, *Waste and Biomass Valorization*, 2021, **12**, 6497-6512.

35. A. Al Ghatta, X. Zhou, G. Casarano, J. Wilton-Ely and J. Hallett, *Acs Sustainable Chemistry & Engineering*, 2021, **9**, 2212-2223.
36. A. Sangregorio, N. Guigo, J. van der Waal and N. Sbirrazzuoli, *Chemsuschem*, 2018, **11**, 4246-4255.
37. J. Pin, N. Guigo, A. Mija, L. Vincent, N. Sbirrazzuoli, J. van der Waal and E. de Jong, *Acs Sustainable Chemistry & Engineering*, 2014, **2**, 2182-2190.
38. A. Sangregorio, N. Guigo, E. de Jong and N. Sbirrazzuoli, *Polymers*, 2019, **11**.
39. Z. Cheng, K. Goulas, N. Rodriguez, B. Saha and D. Vlachos, *Green Chemistry*, 2020, **22**, 2301-2309.
40. H. Shen, H. Shan and L. Liu, *Chemsuschem*, 2020, **13**, 513-519.
41. G. Tsilomelekis, M. Orella, Z. Lin, Z. Cheng, W. Zheng, V. Nikolakis and D. Vlachos, *Green Chemistry*, 2016, **18**, 1983-1993.
42. M. El-Roz, P. Bazin and F. Thibault-Starzyk, *Catalysis Today*, 2013, **205**, 111-119.
43. J. Guo and J. Sun, *Journal of Agricultural and Food Chemistry*, 2002, **50**, 2278-2282.
44. H. WINTER and F. CHAMBON, *Journal of Rheology*, 1986, **30**, 367-382.
45. B. Cheng, X. Wang, Q. Lin, X. Zhang, L. Meng, R. Sun, F. Xin and J. Ren, *Journal of Agricultural and Food Chemistry*, 2018, **66**, 11981-11989.
46. T. Yan, K. Schroter, F. Herbst, W. Binder and T. Thurn-Albrecht, *Macromolecules*, 2017, **50**, 2973-2985.
47. S. Wingstrand, N. Alvarez, Q. Huang and O. Hassager, *Physical Review Letters*, 2015, **115**.
48. M. Denn, J. Morris, J. Prausnitz, M. Doherty and R. Segalman, *Annual Review of Chemical and Biomolecular Engineering, Vol 5*, 2014, **5**, 203-228.
49. S. Bindgen, J. Allard and E. Koos, *Current Opinion in Colloid & Interface Science*, 2022, **58**.
50. M. Quintas, T. Brandao, C. Silva and R. Cunha, *Journal of Food Engineering*, 2006, **77**, 844-852.
51. M. Oroian, S. Amariei, I. Escriche, A. Leahu, C. Damian and G. Gutt, *International Journal of Food Properties*, 2014, **17**, 2228-2240.
52. W. COX and E. MERZ, *Journal of Polymer Science*, 1958, **28**, 619-622.
53. Z. Du, X. Yan, R. Dong, K. Ke, B. Ren and Z. Tong, *Macromolecules*, 2018, **51**, 1518-1528.
54. F. CHAMBON and H. WINTER, *Polymer Bulletin*, 1985, **13**, 499-503.
55. F. CHAMBON, Z. PETROVIC, W. MACKNIGHT and H. WINTER, *Macromolecules*, 1986, **19**, 2146-2149.
56. F. CHAMBON and H. WINTER, *Journal of Rheology*, 1987, **31**, 683-697.
57. L. Tan, D. Pan and N. Pan, *Polymer*, 2008, **49**, 5676-5682.
58. C. Bonino, J. Samorezov, O. Jeon, E. Alsberg and S. Khan, *Soft Matter*, 2011, **7**, 11510-11517.
59. C. Sandolo, P. Matricardi, F. Alhaique and T. Coviello, *Food Hydrocolloids*, 2009, **23**, 210-220.
60. Z. Yang, Y. Hemar, L. Hilliou, E. Gilbert, D. McGillivray, M. Williams and S. Chaieb, *Biomacromolecules*, 2016, **17**, 590-600.
61. M. MUTHUKUMAR and H. WINTER, *Macromolecules*, 1986, **19**, 1284-1285.
62. S. Jungblut, J. Joswig and A. Eychmuller, *Physical Chemistry Chemical Physics*, 2019, **21**, 5723-5729.

63. M. Adam and D. Lairez, *Fractals-Complex Geometry Patterns and Scaling in Nature and Society*, 1993, **1**, 149-169.
64. M. ADAM, D. LAIREZ, F. BOUE, J. BUSNEL, D. DURAND and T. NICOLAI, *Physical Review Letters*, 1991, **67**, 3456-3458.
65. E. Roels, S. Terryn, J. Brancart, R. Verhelle, G. Van Assche and B. Vanderborght, *Soft Robotics*, 2020, **7**, 711-723.
66. K. Cerdan, J. Brancart, H. De Coninck, B. Van Hooreweder, G. Van Assche and P. Van Puyvelde, *European Polymer Journal*, 2022, **175**.
67. S. Seiffert and J. Sprakel, *Chemical Society Reviews*, 2012, **41**, 909-930.
68. M. Davidovich-Pinhas, S. Barbut and A. Marangoni, *Carbohydrate Polymers*, 2015, **117**, 869-878.
69. S. Liu, S. Huang and L. Li, *Journal of Rheology*, 2016, **60**, 203-214.
70. S. Russo Spena, N. Grizzuti and D. Tammaro, *Journal*, 2022, **8**.
71. R. Dinu, S. Montes, F. Orange and A. Mija, *Composites Science and Technology*, 2021, **207**.
72. E. Koos, W. Kannowade and N. Willenbacher, *Rheologica Acta*, 2014, **53**, 947-957.
73. C. Yang, Y. Wang, T. Vasanthan and L. Chen, *Food Hydrocolloids*, 2014, **40**, 225-236.
74. O. Meldrum, G. Yakubov, M. Bonilla, O. Deshmukh, M. McGuckin and M. Gidley, *Scientific Reports*, 2018, **8**.
75. A. Grande, J. Bijleveld, S. Garcia and S. van der Zwaag, *Polymer*, 2016, **96**, 26-34.
76. H. Yang, S. Ghiassinejad, E. van Ruymbeke and C. Fustin, *Macromolecules*, 2020, **53**, 6956-6967.